

Improving the Proton Conductivity and Antibacterial Properties of Sulfonated Polybenzimidazole/ZnO/Cellulose with Surface Functionalized Cellulose/ZnO Bionanocomposites

Ahmadizadegan, Hashem⁺; Esmailzadeh, Sheida[•]; Ranjbar, Mahdi[•]*

Department of Chemistry, Darab Branch, Islamic Azad University, Darab, I.R. IRAN

ABSTRACT: *New bionanocomposite proton exchange membranes were prepared from sulfonated polybenzimidazole (s-PBI) and various amounts of sulfonated ZnO/cellulose nanohybrids (ZnO/cellulose-SO₃H). The use of ZnO/cellulose-SO₃H compensates for the decrease in ion exchange capacity of membranes observed when non-sulfonated nano-fillers are utilized. The strong -SO₃H/-SO₃H interaction between s-PBI chains and ZnO/cellulose-SO₃H hybrids leads to ionic cross-linking in the membrane structure, which increases both the thermal stability and methanol resistance of the membranes. The ZnO/cellulose -SO₃H in the membranes served as spacers for polymer chains to provide extra space for water permeation, so as to bring high permeation rates to the complex membranes. Moreover, the membranes exhibited excellent antibacterial activities against *S. aureus* and *E. coli*. A.*

KEYWORDS: *Sulfonated polybenzimidazole; Proton exchange; ZnO/cellulose; Antibacterial.*

INTRODUCTION

Polybenzimidazole (PBI) is one of the most studied materials for applications in Proton Exchange Membrane Fuel Cell (PEMFC). As PBIs are basic polymers, acid doping in PBIs results in an increase both in their proton conductivities and thermal stability [1, 2]. The effects of acid-doping levels, temperatures, and relative humidity on the proton conductivities of PBI membranes were studied [3–10]. The proton conductivities of acid-doped PBI membranes were also dependent on the doped acids in the order of H₂SO₄ > H₃PO₄ > HClO₄ > HNO₃ > HCl [11]. However, the acids doped in PBI membranes might leak in fuel cell applications. One promising approach to overcome this drawback was to covalently bond the acid

groups, especially sulfonic acid groups, to the PBI chains [12]. The sulfonated PBI membranes showed relatively high proton conductivities comparing to the corresponding pristine PBI membranes. Modification of PEMs to improve their thermal and chemical stability and to depress their methanol crossover is a useful approach to improve their performance. *Yamaguchi et al.* [13] reported pore-filling membranes that were composed of a porous substrate and a filling polyelectrolyte. These pore-filling membranes showed high mechanical strength and low methanol crossover. *Lue et al.* [14] reported that plasma treatment on Nafion[®] surface could change its surface properties substantially with a methanol

* To whom correspondence should be addressed.

+ E-mail: h.ahmadizadegan.2005@gmail.com

• Other Address: Young Researchers and Elite Club, Darab Branch, Islamic Azad University, Islamic Republic of Iran
1021-9986/2018/4/27-42 16/\$/6.06

permeability reduction of 74% and without altering their bulk properties.

Organic–inorganic nanocomposites represent another useful approach to PEM modification [15-17]. It is widely acknowledged that there is a growing need for more environmentally acceptable processes in the chemical industry. This trend towards what has become known as ‘green chemistry’ or ‘sustainable engineering’ needs research on technologies that use preferably renewable raw materials, produce less waste and avoid the use of toxic and hazardous reagents and solvents [18]. Cellulosic materials have also shown some promising applications in the development of alternative energy sources. For example, nanoporous regenerated cellulose membranes have been used in place of proton-exchange membranes in microbial fuel cells [19]. Membranes formed from cellulose acetate and nitrates have also been used extensively in electroanalytical applications [20–22].

In this work, I reported the attempts on preparation of high-performance s-PBI nanocomposite membranes for fuel cell application using sulfonated ZnO/cellulose nanocomposites as nano-reinforcements. S-PBI nanocomposites membranes possessing non-sulfonated ZnO/cellulose nanocomposites were also prepared to study the effects of sulfuric acid groups on the properties of s-PBI nanocomposite membranes. The new membranes were initially synthesized and then the identification of these membranes was performed. Identification of all membranes was carried out successfully. Then a series of the process were performed to identify the properties of these membranes. Based on these data, each section briefly describes each one of the membranes can be used under certain conditions and for specific applications. The sulfuric acid groups of ZnO/cellulose formed ionic linkages with s-PBI chains, improved the compatibility between ZnO/cellulose and s-PBI, and enhance the mechanical strength of the PBI/ZnO/cellulose bionanocomposite membranes. S-PBI/ZnO/cellulose nanocomposite membranes exhibited depressions on methanol permeability and enhancements on proton conductivity comparing to the pristine s-PBI membrane, to promise their application potentials for fuels cells. Moreover, the membranes exhibited excellent antibacterial activities against *S. aureus* and *E. coli*. A.

EXPERIMENTAL SECTION

Materials

2,2-Bis(4-carboxyphenyl)hexafluoropropane, polyphosphoric acid (PPA), N,N-dimethylacetamide (DMAc), sulfuric acid, ethanol, diaminobenzidine reagent, dimethyl sulfoxide (DMSO), and 1,4-bis(hydroxymethyl) benzene (BHMB) were purchased from Aldrich (St. Louis, MO, USA) and used without any purification. ZnO nanoparticles with an average particle size of about 10–15 nm were purchased from Neutrino Co (Tehran, Iran). Research grade ethane, ethylene, propane, and propylene gases (purity 99.95%) were purchased from Technical Gas Service. The Cellulose NanoFibers (CNFs) used in this study were provided by the Institute of Tropical Forestry and Forest Products (INTROP), Malaysia, and were isolated from the kenaf bast fibers (*Hibiscus cannabinus*). The details of the CNFs isolation process are reported elsewhere. The selected fungus was a white rot fungus (*Trametes versicolor*), which was obtained from the National Collection of Biology Laboratory, University of Tehran, Iran. Glycerol, methanol, acetone, acetic anhydride (95%), pyridine, and Malt Extract Agar (MEA) were purchased from the Merck Chemical Co., Germany. All the materials and solvents that were used were obtained from the suppliers without further purification.

Synthesis of ZnO/cellulose bionanocomposites

ZnO/cellulose bionanocomposites was performed using the reported method [23].

Surface-Functionalization of ZnO/cellulose bionanocomposites

The reaction of ZnO/cellulose with Glycidyl Phenyl Ether (GPE) was carried out as follows [24]. The ZnO/cellulose solution and GPE were mixed together. After adding 1000 ppm of SnCl₂ as a catalyst, the mixture was stirred at 130 °C for 6 h. The solvent was removed out with a rotary evaporator, and a condensed product (ZnO/cellulose-GPE) was obtained with centrifugation. The sulfonation on ZnO/cellulose -GPE was carried out with treating ZnO/cellulose-GPE with fuming sulfuric acid. The reaction was performed at room temperature for 20 h. The reaction mixture was poured into plenty of ice-water mixture and the precipitate was collected with a centrifuge. The collected product (ZnO/cellulose -SO₃H)

was then dispersed in an acetic acid aqueous solution to result in a homogeneous solution for further application.

Synthesis of s-PBI polymer

1.28 g diaminobenzidine (6 mmol) and 2, 2-Bis(4-carboxyphenyl)hexafluoropropane (6 mmol) were mixed with PPA (38 g) and placed in a round-bottom flask equipped with a reflux condenser with an inlet for nitrogen. The mixture was heated to 190 °C for 20 h [25]. The polymerized PBI powder was collected and then dissolved in DMAc to prepare 10 wt% of the PBI solution. Incompletely dissolved PBI powder in DMAc was removed by a simple centrifugation step. To improve ion conductivity, the PBI film was treated with 98 wt% sulfuric acid at room temperature for three days (sulfonated-PBI, s-PBI membrane). This s-PBI film was washed with ethanol and subsequently dried at 65 °C for 22 h (Scheme1).

Synthesis of s-PBI/ZnO/cellulose -SO₃H bionanocomposite membrane

ZnO/cellulose-SO₃H (4, 8, 12, 16 and 20 weight% with respect to s-PBI) was suspended in DMAc and vigorously stirred at 30 °C for 24 h. 10% s-PBI by weight was dissolved in the same solution at 60 °C under stirring. The cross-linker, BHMB, was then added at a concentration of 1mol/mol repeat unit in the same solution and stirred till dissolution. The composite solution was then sonicated for 4 h and cast on a glass plate. The film was then dried under ambient conditions for 2 days and then cured under vacuum at different temperatures. The sequence of heating was; 50 °C for 2 h, 100 °C for 2 h, 120 °C for 2 h and 135 °C for 24 h. To compare the properties of the cross-linked s-PBI/ZnO/cellulose-SO₃H bionanocomposite membranes, pure s-PBI and neat 1MBHMB cross-linked membranes were prepared to adopt the same procedure.

Characterization

Fourier-Transform Infrared (FT-IR) spectra were measured on a Nicolet Impact 410 FT-IR spectrometer. Proton Nuclear Magnetic Resonance (¹H-NMR) experiments were carried out on a Bruker 510 spectrometer using deuterated dimethyl sulfoxide as a solvent. Differential Scanning Calorimeter (DSC) measurements were performed on a Mettler Toledo

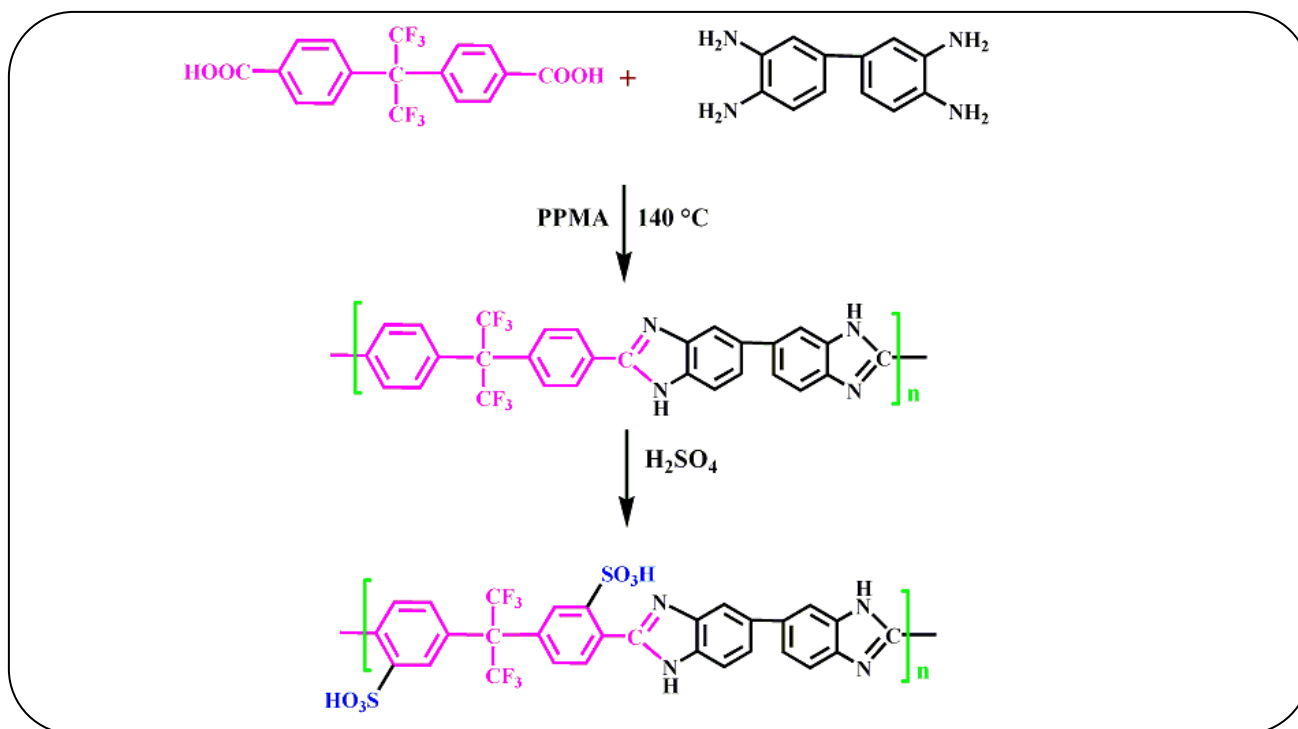
DSC821e instrument at a heating rate of 20°C/min from 80°C to 300°C under nitrogen. Thermo Gravimetric Analysis (TGA) on a PerkinElmer Pyris-1 thermal analyzer system was employed to evaluate the thermal stability of the polymers. To remove water, the membranes were dried and kept in the TGA furnace at 150°C under a nitrogen atmosphere for 15min before testing. The samples were evaluated in the range of 100°C–800°C at a heating rate of 10°C/min under nitrogen atmosphere. Mechanical properties of the membranes were evaluated at room temperature on SHIMADZU AG-I 1KN at a strain rate of 2 mm/min, and a 500 N load cell was used. The samples were prepared by cutting the membranes in dumbbell shapes of 15 mm × 4 mm. At least three measurements for each membrane were taken and the average value calculated. The oxidative stability of the membranes was evaluated by immersing the samples in a Fenton's reagent (3% hydrogen peroxide (H₂O₂) containing 2 ppm ferrous sulfate (FeSO₄)) at 80°C. The stability was evaluated by recording the time when the membranes begin to break into pieces and start disappearing. The gas permeability of the polymer membranes with thickness around 30 μm was measured with an automated Diffusion Permeameter (DP-100-A) manufactured by Porous Materials Inc., USA, which consists of upstream and downstream parts separated by a membrane. Elemental analysis on carbon was conducted with a Heraeus CHN-O rapid elementary analyzer with benzoic acid as a standard. Scanning electron micrographs were observed with a Hitachi S-3000N Hi-SEM. Energy Dispersive X-ray (EDX) measurements were conducted with a Horiba ES-320 Energy Dispersive X-Ray Micro Analyzer.

Water uptake and acid-doping level

Water uptake measurement was performed by dipping the dried membranes (dried at 120 °C in vacuo for 5 h) in distilled water for 24h at 25 or 80°C. The membranes were taken out, wiped with paper, and then weighted. The water uptake was calculated by Eq. (1):

$$\text{Water uptake(\%)} = \frac{W_s - W_d}{W_d} \quad (1)$$

Where W_s and W_d are membrane weights after and before dipping, respectively. Acid-doping level was obtained in a similar manner. Membranes were dipped in an 85% H₃PO₄ solution for 1 week at room temperature.



Scheme 1: Synthesis of the fluorine-containing s-PBI copolymer.

To exclude the weight gain due to water uptake, doped membranes were dried at $110\text{ }^\circ\text{C}$ under vacuum until the membrane weights unchanged with time. The weight change in acid doping was measured and used for the calculation of acid doping level (acid numbers per s-PBI repeating unit).

Methanol permeability

Methanol permeability measurement was performed on a two-reservoir compartment in which the membrane was clamped between the two reservoirs. The membranes were hydrated in deionized water at room temperature for 24 h prior to measurement.

Source cell ($V_A = 20\text{ mL}$) was filled with a 3-M methanol aqueous solution, and receiving cell ($V_B = 18\text{ mL}$) was filled with deionized water. The concentration of methanol in receiving cell was measured versus time by gas chromatography GC390B (CL Sciences Inc., Japan) with a gas flow rate of 30 mL/min . The methanol concentration of the source cell was considered much higher than that of the receiving cell during measurements. Methanol permeability was calculated by Eq. (2):

$$CB(t) = \frac{A \times D \times K}{V_B \times L} C_A (t - t_0) \quad (2)$$

where C_B is the methanol concentration in receiving cell, C_A the initial methanol concentration, A the cross-section area, L the membrane thickness, D the methanol diffusivity and K the partition coefficient. The product DK is the membrane permeability to methanol. Parameter t_0 is the "lag time" corresponding to the time necessary for the methanol to pass through the membrane.

Proton conductivity

The proton conductivity of the membranes was measured with a Solartron 1255B frequency response analyzer equipped with a Solartron 1287 electrochemical interface with an oscillation amplitude of 10 mV and a frequency range of 0.1 Hz to 1 MHz .

The measurements were taken at $20\text{--}80\text{ }^\circ\text{C}$ under a 95% relative humidity.

Testing of Antibacterial Activity

The antibacterial activity of the pure s-PBI and s-PBI/ZnO/cellulose- SO_3H films was examined using the disc diffusion method and colony-forming count method for qualitative and quantitative analyses, respectively. The gram-positive bacterium *Staphylococcus aureus* (*S. aureus*) and gram-negative bacterium *Escherichia coli*

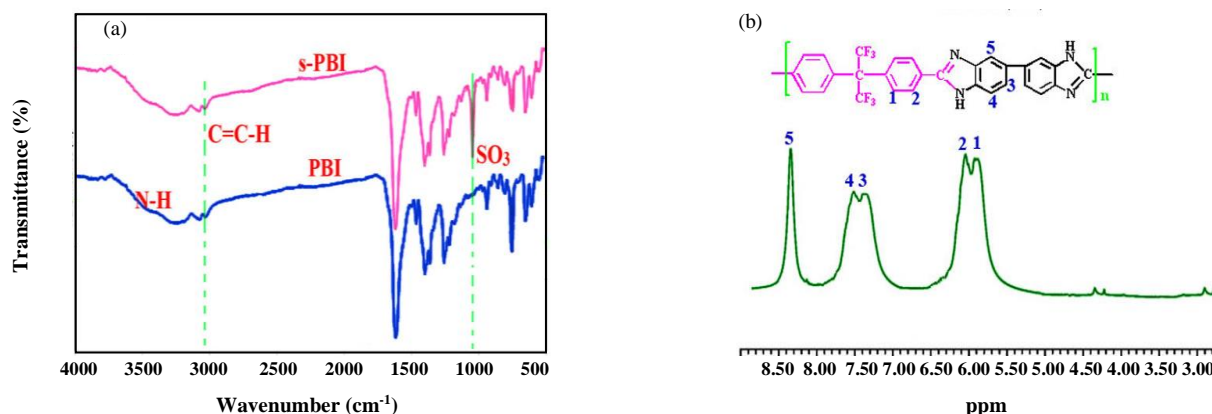


Fig. 1 (a) Fourier transforms infrared (FT-IR) spectra of polybenzimidazole (PBI) and sulfonated PBI (s-PBI) and (b) $^1\text{H-NMR}$ (500 MHz) spectrum of PBI at RT.

(*E. coli*) were administered; the final concentrations of the bacterium were 1.0×10^8 and 3.0×10^8 CFU/mL, respectively. The bacteria were all ATCC. The disc diffusion method was performed using Luria-Bertani (LB) medium solid agar in Petri dishes. Pure s-PBI and s-PBI/ZnO/cellulose-SO₃H films were cut into 6 mm pieces sterilized by UV light and placed on *S. aureus*-cultured agar and *E. coli*-cultured agar plates, which were then incubated at 37 °C for 24 h. After incubation, a bacterial inhibition zone formed around the film. The width of the inhibition zone (W_{inh}) was calculated using the following equation: [26]

$$W_{\text{inh}} = \frac{d_1 - d_2}{2}$$

Where d_1 is the total diameter of the inhibition zone and the film, and d_2 is the diameter of the film (6 mm).

In the colony-forming count method, three pieces of pure s-PBI or s-PBI/ZnO/cellulose-SO₃H films (1 cm × 1 cm) were sterilized by UV light and then immersed in 10 mL of the bacterial suspension in an Erlenmeyer flask. The solution was then shaken at 200 rpm at 37 °C. Viable cell counts of the bacteria were obtained using the surface spread plate method. At 0, 1, 3 and 6 h intervals, 0.2 mL of bacterial culture was taken from the flask and serial dilutions were repeated with PBS in each initial sample, respectively. 0.1 mL diluent of the sample was then spread onto solid growth agar plates. The plates were incubated at 37 °C for 24 h, and the number of viable cells was manually counted and then multiplied by the dilution factor.

RESULTS AND DISCUSSION

FT-IR of PBI and s-PBI Membranes

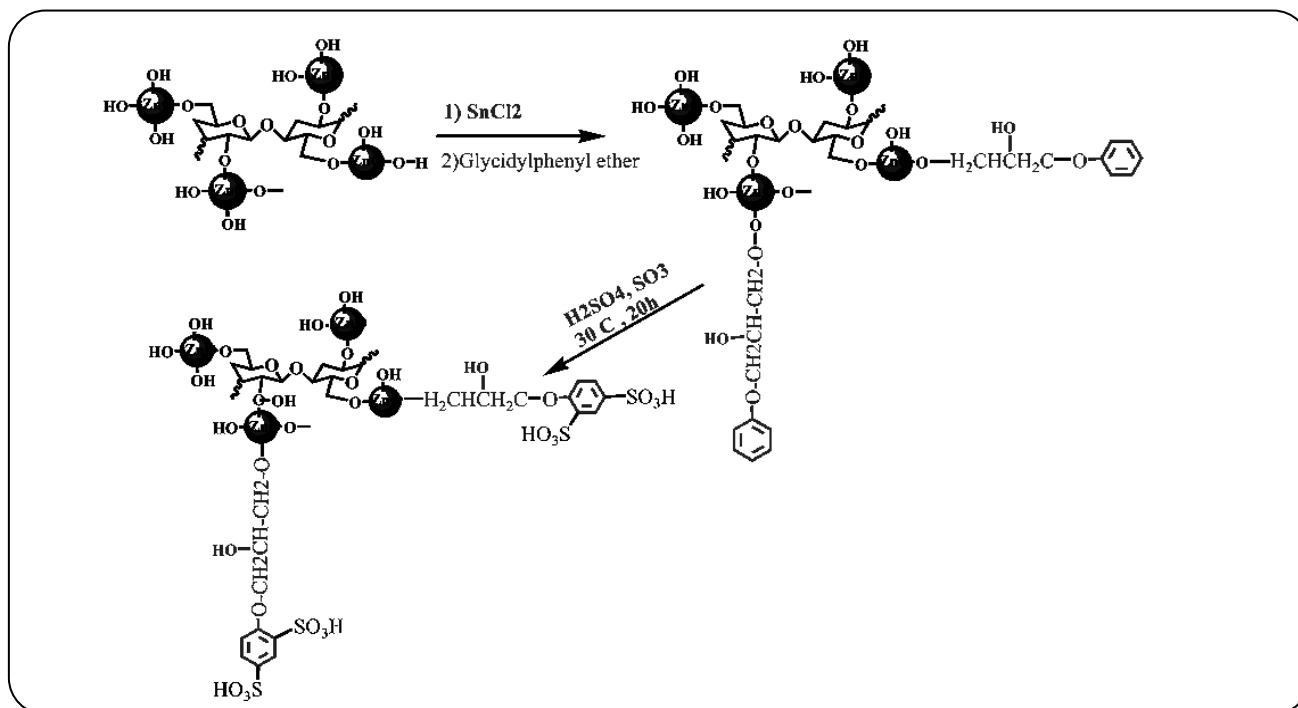
Fig. 1(a) shows the infrared (IR) spectra of PBI and s-PBI with characteristic peaks at 3200–3500 cm⁻¹ for the N–H bond and at 1645 cm⁻¹ for the C=N bond, respectively. The distinctive in-plane deformation peak of the imidazole ring was also observed at 1450 cm⁻¹. Upon sulfonation, the s-PBI membrane clearly showed a new broad peak at 1050 cm⁻¹, corresponding to the symmetric stretch of the sulfonate group (SO₃⁻).

$^1\text{H NMR}$ spectrum of PBI

$^1\text{H NMR}$ spectrum of PBI is shown in Fig. 1(b). All protons from 5.8 to 7.9 ppm with expected multiples and integrations are consistent with the proposed chemical structures of PBI. The signal of –NH in the imidazole ring was not obvious due to a strong proton exchange with the trace amount of water in the solvent. All other protons had very good correspondence and attribution. In addition, the chemical structure of PBI was also confirmed by its $^1\text{H NMR}$ spectrum (Fig 1(b)), which was consistent with the proposed chemical structures of PBI.

Preparation of sulfonic acid functionalized ZnO/cellulose bionanocomposite

The surfaces of nanoscale ZnO/cellulose composites were functionalized with the sulfonic acid group via a two-step reaction, as shown in scheme 2. First, the nanoscale ZnO/cellulose composites were reacted with glycidyl phenyl ether through the addition reaction between Zn–OH, CH₂–OH of cellulose and oxirane group to result



Scheme 2: surfaces functionalized of nanoscale ZnO/cellulose composites with a sulfonic acid group.

in ZnO/cellulose composites with phenyl pendent groups on their surface (ZnO/cellulose-GPE).[24] Subsequently, sulfonation on the pendent phenyl groups on the ZnO/cellulose composites surface was performed by treating the obtained ZnO/cellulose-GPE with fuming sulfuric acid through the electrophilic substitution reaction. The functionalization reaction and the chemical structure of the ZnO/cellulose were characterized with FT-IR. Based on the FT-IR spectrum of ZnO/cellulose-GPE, the occurrence of the reaction between the Zn-OH, CH₂-OH of cellulose group and oxirane ring was observed with the disappearance of the absorption peak at 915 cm⁻¹ (oxirane ring). With the presence of absorption bands at 1647 and 1523 cm⁻¹ (phenyl ring), 2865 cm⁻¹ (C-H stretching in methylene group), and 3015 cm⁻¹ (aromatic C-H stretching), it was confirmed that the glycidyl phenyl ether groups were covalently incorporated onto the ZnO/cellulose composites. Moreover, strong absorption at 1169 cm⁻¹ (-SO₃H) and 610 cm⁻¹ (-C-S) were observed for ZnO/cellulose-SO₃H. This indicates that the occurrence of sulfonation reaction and the introduction of -SO₃H groups onto the GPE moieties of ZnO/cellulose-GPE were achieved.

The carbon contents of ZnO/cellulose-GPE and ZnO/cellulose-SO₃H were found to be 21.85 and 8.77 wt%,

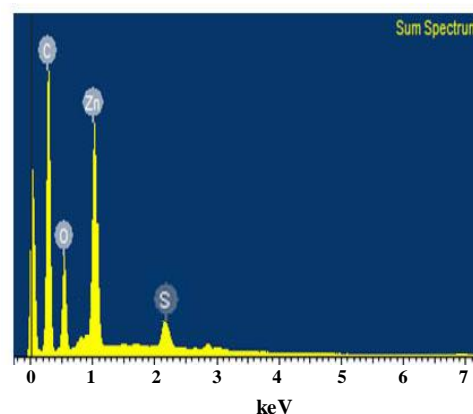


Fig. 2: EDX spectrum for elemental analysis on ZnO/cellulose-SO₃H.

respectively. The value of the carbon content of ZnO/cellulose-SO₃H was coincident to the calculated one. This further demonstrates that the Zn-GPE and CH₂-GPE linkages were sustainable under the conditions of sulfonation reaction. The successful incorporation of GPE onto the nanoscale ZnO/cellulose composites and the sulfonation on the composites were also demonstrated with Energy-Dispersive X-ray (EDX) spectroscopy. As shown in Fig. 2, the incorporation of GPE moieties were directly observed from the presence of the carbon

absorption peak. Moreover, the sulfur peak that appeared in the EDX spectrum of ZnO/cellulose-SO₃H confirmed the occurrence of the sulfonation reaction on the aromatic groups.

Characterizations on s-PBI nanocomposite membranes

S-PBI and ZnO/cellulose-SO₃H were prepared in our laboratory. S-PBI and ZnO/cellulose-SO₃H could form homogeneous solutions. The s-PBI/ZnO/cellulose-SO₃H bionanocomposites membranes were therefore obtained with a casting method. S-PBI/ZnO/cellulose membranes were also prepared with uses of non-sulfonated ZnO/cellulose to replace ZnO/cellulose-SO₃H to examine the effect of sulfonic acid groups on the properties and performances of the s-PBI nanocomposites membranes. Fig. 3 shows the SEM micrographs of the s-PBI/ZnO/cellulose nanocomposite membranes. Pure s-PBI membranes exhibited dense and homogeneous morphology for both surfaces (Fig. 3a). The ZnO/cellulose composites in s-PBI/ZnO/cellulose (16%) membrane could be seen in its surface SEM micrograph (Fig. 3b). Particles in sizes of about 33nm aggregate together to form ZnO/cellulose domains in micrometers, indicating the interactions between ZnO/cellulose nanocomposites are stronger than that between s-PBI molecules and ZnO/cellulose nanocomposites. The agglomerated ZnO/cellulose domains were also observed in the cross-sectional SEM micrograph of PBI/ZnO/cellulose (16%) (Fig. 3c). The SEM observations indicate that the compatibility between s-PBI and ZnO/cellulose nanocomposites and the homogeneity of the s-PBI/ZnO/cellulose membranes are somewhat poor. However, the dispersion homogeneity of ZnO/cellulose nanocomposites in s-PBI membranes could be significantly improved with using ZnO/cellulose-SO₃H as the additives. As shown in Fig. 3d, isolated ZnO/cellulose composites were observed in the surface SEM micrograph of s-PBI/ZnO/cellulose-SO₃H bionanocomposite membranes, demonstrating the high compatibility between s-PBI polymer and ZnO/cellulose-SO₃H composites and the high dispersion ability of ZnO/cellulose-SO₃H in s-PBI matrix. Particle agglomeration was still not observed in the cross-sectional SEM micrograph of s-PBI/ZnO/cellulose-SO₃H (16%) (Fig. 3e). s-PBI has a pK_a value of about 4.2. The basicity of s-PBI makes it readily reactive toward the sulfonic acid groups of ZnO/cellulose-SO₃H through ionic interaction. The ionic linkages between s-PBI

and ZnO/cellulose-SO₃H contribute to their high compatibility. Fig. 3 shows the SEM-EDX elemental mapping micrographs of s-PBI/ZnO/cellulose-SO₃H (20%). ZnO and sulfur elements were observed to demonstrate the presence of ZnO/cellulose-SO₃H particles in s-PBI bionanocomposite membranes. In addition, the distributions of ZnO and sulfur in the micrographs are homogeneous, indicating that there was not particle agglomeration and micro-phase separation in the bionanocomposites membranes. Therefore, ZnO/cellulose-SO₃H composites could be considered homogeneously dispersing in the s-PBI polymer matrix.

The FT-IR spectra of s-PBI and its bionanocomposites showed absorption peaks at 3445 and 3245cm⁻¹ correspond to the non-hydrogen bonded N-H stretching and hydrogen bonded (self-associated) N-H groups, respectively. The absorption peaks at 1455 and 1550cm⁻¹ arise from the in-plane deformation of benzimidazole, and the peak at 1290cm⁻¹ is from the breathing mode of imidazole rings. The absorption peak at about 1155cm⁻¹ in relatively low intensity might correspond to the in-plane C-H deformation vibrations [27]. After addition of ZnO/cellulose nanocomposites, the absorption intensities at about 1120cm⁻¹ increased due to the contribution of Zn-O-Zn absorption. The result indicates the presence of ZnO/cellulose in both s-PBI/ZnO/cellulose (16%) and s-PBI/ZnO/cellulose-SO₃H (16%) nanocomposite membranes. In addition, s-PBI/ZnO/cellulose-SO₃H (16%) exhibited some minor absorption peaks at 1360 and 1152cm⁻¹ corresponding to the absorptions from the sulfuric acid groups. A decrease in the relative intensity of absorption peak at 3444cm⁻¹ was observed with s-PBI/ZnO/cellulose-SO₃H (16%), indicating some of the non-hydrogen bonded N-H groups in PBI chains bond to the sulfonic acid groups of ZnO/cellulose-SO₃H (16%) via H-bonding and ionic interaction.

The diagram in Fig. 5 is calculated from 300 ° C, in the previous steps, there were two failures in the diagram that corresponds to both losses of H₂O and SO₃H. The first step of degradation in pure s-PBI at about 110 °C is due to the loss of water molecules absorbed by the highly hygroscopic SO₃H groups. The second weight loss that started around 255 °C was assigned to the degradation of SO₃H groups [28].

The glass transition temperatures (T_g) of s-PBI/ZnO/cellulose-SO₃H bionanocomposite membranes

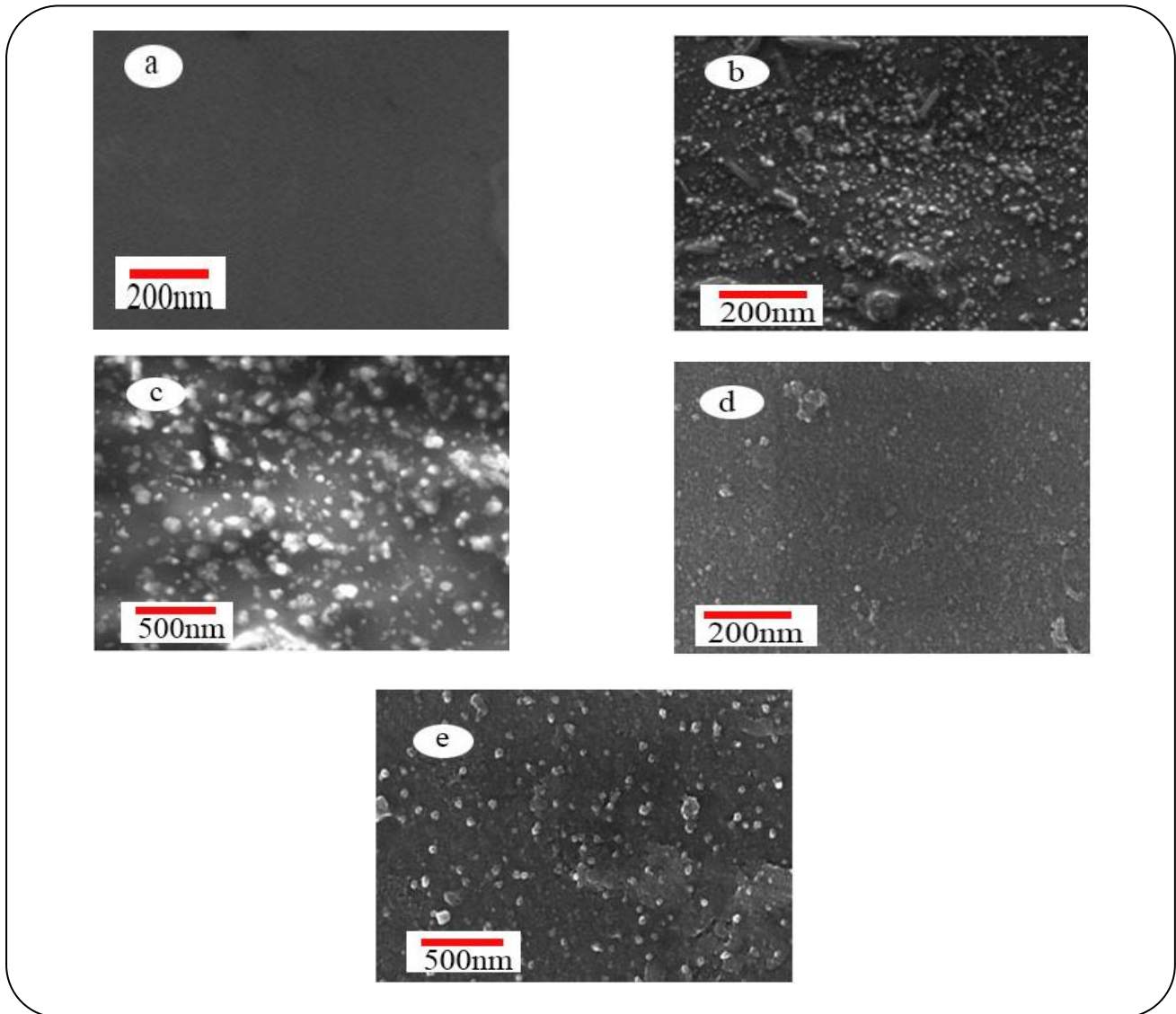


Fig. 3: SEM micrographs of s-PBI (a) surface and its nanocomposites of s-PBI/ZnO/cellulose (16%) ((b) surface and (c) cross-section) and s-PBI/ZnO/cellulose-SO₃H (16%) ((d) surface and (e) cross-section).

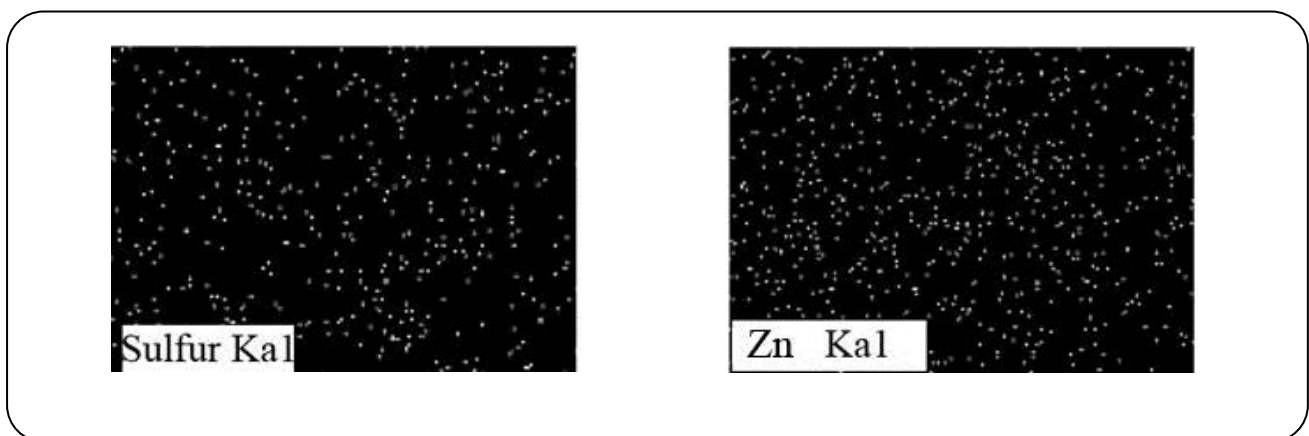


Fig. 4: EDX mapping results of s-PBI/ZnO/cellulose-SO₃H: S-mapping (Ka1) and Zn-mapping (Ka1).

were read from the $\tan \delta$ peaks in DMA thermograms (figures not shown). Pure s-PBI showed a T_g of 386 °C, which shifted to higher temperatures (475–480 °C) while the formation of nanocomposites with ZnO/cellulose-SO₃H. The T_g increase indicates that the motion ability of s-PBI chains is restricted with the presence of being majorly contributed from the strong ionic linkages between s-PBI and ZnO/cellulose-SO₃H. The ionic linkages ZnO/cellulose-SO₃H. The chain motion restriction should bring a cross-linking effect to the s-PBI/ZnO/cellulose-SO₃H nanocomposite membranes, so as to increase the T_g s of the s-PBI/ZnO/cellulose-SO₃H nanocomposites. The contributions of –SO₃H/–NH and –SO₃H/–SO₃H ionic linkages to T_g enhancement was also demonstrated with the relatively low T_g of s-PBI/ZnO/cellulose-(20%) (430 °C), as ZnO/cellulose does not possess sulfonic acid groups. On the other hand, the presence of ZnO/cellulose or ZnO/cellulose-SO₃H did not significantly alter the thermal degradation behaviors of s-PBI polymer, as shown with their TGA thermograms (Fig. 4). The –SO₃H/–NH and –SO₃H/–SO₃H ionic linkages in the ZnO/cellulose-SO₃H/s-PBI nanocomposites membranes broke down before the degradation of s-PBI chains. Due to the presence of the ZnO/cellulose nanocomposites did not involve in the degradation reactions of polymer portion [27, 29], all s-PBI/ZnO/cellulose-SO₃H nanocomposites as well as s-PBI polymer exhibited similar degradation temperatures, which was due to the degradation of s-PBI chains. However, the presence of inorganic portions in the s-PBI nanocomposite membranes might reduce the weight loss rate of the s-PBI nanocomposites in the high-temperature region and increase the char yields of the nanocomposites. The relatively high char yield of s-PBI/ZnO/cellulose-SO₃H (20%), compared to that of s-PBI/ZnO/cellulose (20%), is attributed to the promoting effect of sulfonic acid groups on the dehydration/carbonization during s-PBI thermal degradation.

The mechanical properties of the s-PBI-based membranes were measured with an Instron. The stress-strain curves are shown in Fig. 5. Pure s-PBI membrane showed Young's modulus of 3.1 GPa and an elongation at break of 50%. Formation of nanocomposites with ZnO/cellulose composites results in increases in tensile strengths and decreases in elongations at the break for the s-PBI-based membranes. For s-PBI/ZnO/cellulose-SO₃H

nanocomposites membranes, the presence of ionic linkages between s-PBI and ZnO particles attributes to their high Young's modulus, especially for high ZnO/cellulose-SO₃H loaded samples of s-PBI/ZnO/cellulose-SO₃H (16%) and s-PBI/ZnO/cellulose-SO₃H (20%) (Young's modulus above 4.2MPa). Introduction of ZnO/cellulose-SO₃H increased the brittleness of the s-PBI-based membranes with the decreases in their elongations at break. The brittleness of the membranes increased with increasing their ZnO/cellulose contents. The effects of ZnO/cellulose and ZnO/cellulose-SO₃H on the elongations at break of the nanocomposite membranes were similar. The decreases in the elongation at break and increases in the brittleness were widely observed with polymer nanocomposites and could be attributed to the presence of inorganic reinforcement [30].

Moreover, the ionic linkages in s-PBI/ZnO/cellulose-SO₃H as well as the hydrogen bonding in s-PBI/ZnO/cellulose also bring some cross-linking effect to the s-PBI chains so as to decrease the elongation at break of the polymer. Therefore, the s-PBI/ZnO/cellulose-SO₃H membranes could be superior to the s-PBI/ZnO/cellulose membranes in mechanical characteristics. Moreover, the high brittleness of s-PBI/ZnO/cellulose (20%) and s-PBI/ZnO/cellulose-SO₃H (20%) (possessing 10% of the elongation at break) might limit their applications for fuel cell membranes. Comparatively, s-PBI/ZnO/cellulose-SO₃H (16%), which showed an elongation at break of 18%, is more suitable for the membrane applications. S-PBI exhibits water uptake of 18.6% at 25 °C, corresponding to 3.24 molecules of water associating with one s-PBI repeating unit.

Water uptake of s-PBI bionanocomposites

The measured value of water uptake is reasonable comparing to the proposed values by Li et al. [5], who suggested that N atom and N–H groups in s-PBI repeating units formed intermolecular hydrogen bonds with 2–4 water molecules. Addition of ZnO/cellulose nanocomposites to s-PBI membranes increased their water uptakes (Fig. 7) due to the hygroscopic nature of ZnO/cellulose nanocomposites. The sulfonic acid groups in ZnO/cellulose-SO₃H nanocomposites further increased the water uptakes to greater extents. S-PBI/ZnO/cellulose

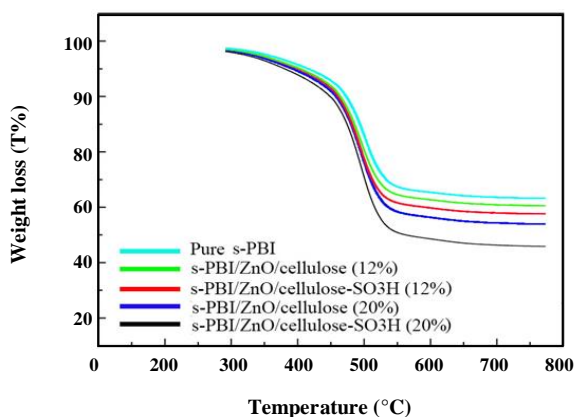


Fig. 5: TGA thermograms of s-PBI-based membranes and nanocomposites.

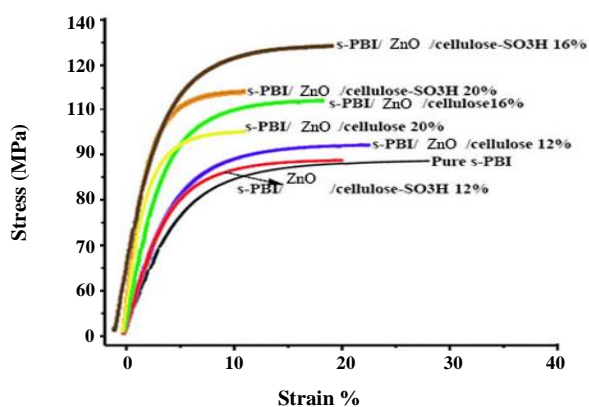


Fig. 6: Stress-strain curves of the nanocomposite membranes.

(20%) and s-PBI/ZnO/cellulose-SO₃H (20%) showed water uptake of 22.9 and 25.6 wt% at 25 °C, respectively. Besides, the water uptakes of the s-PBI-based membranes measured at 25 °C were higher than the values measured at 80 °C. Ying-Ling Liu *et al.* [27] reported that PBI polymer chain shrank in DMAc at elevated temperature, which was caused by disruption of interchain hydrogen bonding, and underwent a conformational change from extended helical conformer to collapsed compact coil conformer. The low water uptakes observed with s-PBI membranes at high temperatures might be attributed to the s-PBI chain shrinkages in water. Similar results were also reported with Qing *et al.* [13, 14] for s-PBI polymers. The s-PBI-based membranes were doped with 85% H₃PO₄ to prepare the acid-doped membranes for fuel cell applications. Fig. 8 shows the acid-doping levels of the s-PBI-based nanocomposite membranes. Acid-doping level (H₃PO₄ molecules per s-PBI repeating unit)

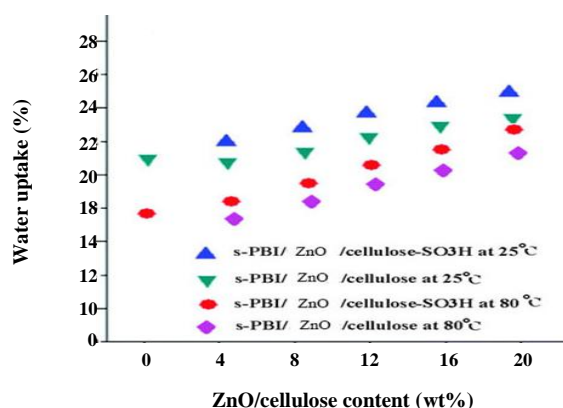


Fig. 7: Water uptakes of the s-PBI nanocomposite membranes.

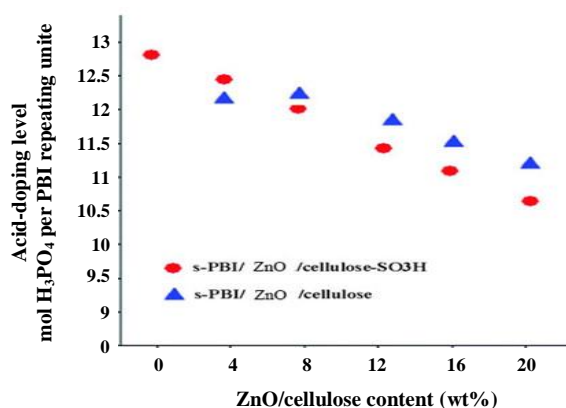


Fig. 8: Acid-doping levels of s-PBI nanocomposite membranes with H₃PO₄.

of the pure s-PBI membrane was 12.6, which decreased to 10.1 and 9.7 for s-PBI/ZnO/cellulose (20%) and s-PBI/ZnO/cellulose-SO₃H (20%), respectively (Fig. 8). Some of the amino groups in s-PBI chains were blocked with the sulfonic acid groups of ZnO/cellulose-SO₃H, to decrease the binding ability of s-PBI chains to H₃PO₄ molecules. Although high acid-doping levels are expected for fuel cell applications, these prepared s-PBI nanocomposites membranes still showed high proton conductivities, to be discussed below. In the case of membranes without SO₃H in scheme 2: the -NH groups of s-PBI chains and hydroxyl groups in the surface structure of ZnO/cellulose nanocomposites can be locked and because of due to more acidic hydrogen in SO₃H group so, it reduced with more intensity. But in the case of membranes without SO₃H, because they have only O-H groups (surface structure of ZnO/cellulose), then with less acidic intensity, it reduced with less intensity.

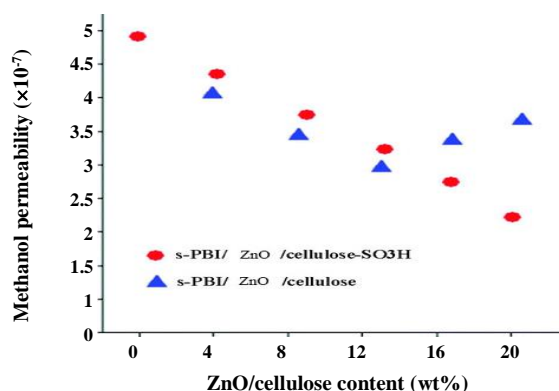


Fig. 9: Methanol permeability of s-PBI bionanocomposite membranes.

Methanol permeability and proton conductivity of s-PBI nanocomposite membranes

The methanol permeability of s-PBI-based membranes was measured with a 3-M methanol aqueous solution at 25 °C by a side-by-side method. Pure s-PBI membrane (without acid doping) exhibited a methanol permeability of 1.78×10^{-9} cm²/s, which increased to 4.98×10^{-7} cm²/s after being doped with H₃PO₄. The protonation of s-PBI chains with acid doping reduced the intermolecular interaction forces of s-PBI and increased the free volume of s-PBI, consequently to generate some additional spaces for methanol crossing the s-PBI membrane. The presence of ZnO/cellulose composites in the s-PBI nanocomposite membranes played some counteraction to this effect. As shown in Fig. 9, the s-PBI nanocomposites exhibited relatively low methanol permeability. The increases in methanol permeability of s-PBI/ZnO/cellulose (16%) and s-PBI/ZnO/cellulose (20%) membranes could be due to the poor compatibility between s-PBI and ZnO/cellulose composites and the agglomeration of ZnO/celluloses in the s-PBI/ZnO/cellulose nanocomposites membranes. Since ZnO/cellulose composites are much compatible with s-PBI, the continuing decreases in the methanol permeability were reasonably observed with s-PBI/ZnO/cellulose-SO₃H (16%) and s-PBI/ZnO/cellulose-SO₃H (20%). It is noteworthy that the methanol permeability of s-PBI/ZnO/cellulose-SO₃H (20%) membrane (2.2×10^{-7} cm²/s) is about near the value read with Nafion[®] (3.7×10^{-6} cm²/s) [31].

The proton conductivities of the phosphoric acid-doped s-PBI membranes at 95% relative humidity as a function of temperatures are shown in Table 1.

The proton conductivities of all membranes increased with increasing the operating temperatures.

Addition of the un-modified ZnO/cellulose showed a negative effect on the proton conductivities of the s-PBI/ZnO/cellulose membranes. On the other hand, compared to the pure s-PBI and Nafion[®] 117 membranes, the relatively high proton conductivities of the s-PBI/ZnO/cellulose-SO₃H nanocomposites membranes are noteworthy. Li *et al.* [31] used sulfonated organosilica to modify Nafion[®] membranes and they found the proton conductivities of the modified membranes were still lower than that of the neat Nafion[®] membrane.

The reduction in the proton conductivity was attributed to the ZnO/cellulose-SO₃H-induced changes in the tortuous paths and in the distribution of hydrophilic/hydrophobic domains. However, in this work an enhancing effect on the proton conductivity was observed with the addition of sulfonated ZnO/cellulose nanocomposites to s-PBI membranes. High proton conductivities were observed with the s-PBI/ZnO/cellulose-SO₃H nanocomposites membranes, even the membranes possessed relatively low acid-doping levels comparing to the pure s-PBI membrane. High doping levels have been recognized to result in high proton conductivities for H₃PO₄-doped s-PBI membranes, due to the excess H₃PO₄ could form anion pathways for proton conduction [4]. However, the H₃PO₄ doping levels of the s-PBI/ZnO/cellulose-SO₃H membranes were still high enough for proton conduction [31]. The sulfonic acid groups of ZnO/cellulose-SO₃H also contribute to the acid-doping effect to s-PBI polymer so as to enhance the proton conductivity of s-PBI/ZnO/cellulose-SO₃H nanocomposites membranes [12–14]. Moreover, the presence of ZnO/cellulose-SO₃H composites induced proton conductive pathways attributing to the increases in the proton conductivities of s-PBI/ZnO/cellulose-SO₃H membranes. The proton conductivities of the acid-doped s-PBI/ZnO/cellulose-SO₃H nanocomposites membranes were further studied at high temperatures under an anhydrous environment (Table 2). All the s-PBI/ZnO/cellulose-SO₃H nanocomposite membranes still exhibited higher proton conductivities that did the pure acid-doped s-PBI membrane. Since the Grothuss-type diffusion mechanism without the assistance of the vehicle, the mechanism has been proposed for the proton conduction

Table 1: The proton conductivities of the phosphoric acid-doped s-PBI membranes at 95% relative humidity as a function of temperatures.

materials	Temperatures °C			
	25	45	65	85
Pure s-PBI	0.010	0.011	0.013	0.016
s-PBI/ZnO/cellulose-SO ₃ H (8%)	0.018	0.020	0.021	0.023
s-PBI/ZnO/cellulose-SO ₃ H (16%)	0.038	0.031	0.029	0.027
s-PBI/ZnO/cellulose-SO ₃ H (20%)	0.016	0.019	0.021	0.023
s-PBI/ZnO/cellulose (8%)	0.001	0.003	0.005	0.008
s-PBI/ZnO/cellulose (16%)	0.008	0.010	0.011	0.013
s-PBI/ZnO/cellulose (20%)	0.010	0.013	0.015	0.022
Nafion® 117	0.045	0.053	0.064	0.084

Table 2" Proton conductivities of s-PBI/ZnO/cellulose-SO₃H doped membranes at high temperature region and under dry environment.

materials	Temperatures °C			
	100	120	140	160
Pure s-PBI	0.0013	0.0014	0.0016	0.0017
s-PBI/ZnO/cellulose-SO ₃ H (4%)	0.0030	0.0037	0.0040	0.0036
s-PBI/ZnO/cellulose-SO ₃ H (8%)	0.0045	0.0046	0.0046	0.0047
s-PBI/ZnO/cellulose-SO ₃ H (12%)	0.0053	0.0060	0.0060	0.0062
s-PBI/ZnO/cellulose-SO ₃ H (16%)	0.0041	0.0059	0.0060	0.0060
s-PBI/ZnO/cellulose-SO ₃ H (20%)	0.0044	0.0050	0.0051	0.0052
Nafion® 117	0.0026	0.0011	0.0001	0.0001

under anhydrous environments [3, 10], the proton conductivity of the acid-doped s-PBI/ZnO/cellulose-SO₃H membranes could be synergistically resulted from their ZnO/cellulose-SO₃H contents and the acid-doping levels. Consequently, the highest proton conductivity was obtained with the acid-doped s-PBI/ZnO/cellulose-SO₃H (12%) membrane, which possesses the moderate ZnO/cellulose-SO₃H content and acid-doping level. It is noteworthy that Nafion® 117 shows relatively low proton conductivities under the anhydrous condition and almost loses its proton conductivities at high temperatures. Comparing to Nafion® 117 membranes, the high proton

conductivities of s-PBI/ZnO/cellulose-SO₃H (12%) indicate that this membrane could be utilized as proton exchange membranes for fuel cells at high temperatures and dry conditions.

The high proton conductivities and low methanol permeability of the s-PBI/ZnO/cellulose-SO₃H nanocomposite membranes indicate their potentials of applications as the proton exchange membranes in direct methanol fuel cells (DMFC), which are evaluated with the membrane selectivity, i.e. the ratio of the proton conductivity to the methanol permeability [32]. The relative selectivity of the s-PBI-based membrane is higher

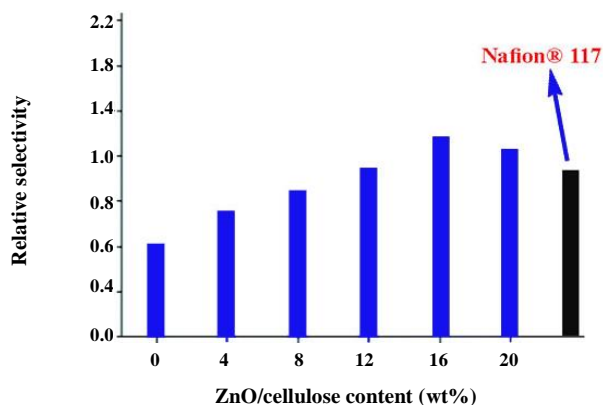


Fig. 10: The relative selectivity (over the Nafion® 117 membrane) of membranes of s-PBI and sulfonated ZnO/cellulose nanocomposites.

than or comparable to that of the Nafion® 117 membrane as shown in Fig. 10. S-PBI/ZnO/cellulose-SO₃H (16%) membrane shows the highest selectivity among the evaluated membranes, which is of about 1.5-folds of the selectivity of the Nafion® 117 membranes. Moreover, the s-PBI/ZnO/cellulose-SO₃H membranes could be highly superior over the Nafion® 117 membrane at high temperatures and dry conditions, since under this operating condition the Nafion® 117 membrane shows a very low selectivity.

Antibacterial Properties

Fig. 11 shows the inhibition zone test of the films against *E. coli*. and *S. aureus*. S-PBI films did not indicate any detectable inhibition zones. In contrast, significant inhibition zones were observed for s-PBI/ZnO/cellulose-SO₃H membranes. The width of the inhibition zone around s-PBI/ZnO/cellulose-SO₃H films showed significant growth with increased ZnO/cellulose-SO₃H content for both *S. aureus* and *E. coli* after one day, varying in the range of 5.4-12.2 mm and 4.1-10.8 mm, respectively. Moreover, the nanocomposite films demonstrated a stronger influence on *S. aureus* than *E. coli*. The results are in agreement with previously reported literature [33-35]. The nature of the cell wall structure is one of the possible reasons for different sensitivity [36].

S. aureus is composed of multi-layers of peptidoglycan with an abundant amount of pores that renders them more susceptible to reactive species, leading to cell disruption. The cell wall of *E. coli* is relatively

thin and is mainly comprised of peptidoglycan, while the outer layer consists of lipopolysaccharide, lipoprotein, and phospholipids, which would be less vulnerable to the attack of a reactive species. Therefore, bionanocomposites films displayed better antibacterial activity against *S. aureus* than *E. coli*. The antibacterial properties of bionanocomposites films were also quantitatively evaluated using the colony-forming count method (Fig. 12). S-PBI films did not demonstrate any antibacterial activity for *E. coli* and *S. aureus*, and the number of viable bacteria remained static. However, a 5-log reduction and 6-log reduction in the viable bacteria of *E. coli* were observed within 2 h of exposure in bionanocomposites (8%) and bionanocomposites (20%) films (Fig. 14a), respectively. When the contact time increased to 4 h, a more significant reduction in the viable bacteria of *E. coli* was observed for bionanocomposites (8%) (7.5-log) and bionanocomposites (20%) films (9-log). After 6 h of exposure, the *E. coli* bacteria were completely eradicated. As shown in Fig. 14b, bionanocomposites films showed more rapid sterilization for *S. aureus* than *E. coli*. After 2 h of treatment, a 7-log and 9-log reduction was observed for *S. aureus* in bionanocomposites (8%) and bionanocomposites (20%) films, respectively. And a 90% reduction in viability was reached after 4 h for the bionanocomposites (20%) film. Enhanced antibacterial properties were identified in bionanocomposites films could be attributed to the porous structure of bionanocomposites films and the enhanced dispersion stability of ZnO/cellulose nanocomposites in the s-PBI matrix.[36] The porous structure provided empty space that allowed the water molecules to react with the incorporated ZnO/cellulose composites, leading to the generation of reactive species, such as oxy-radical or hydroxyl-radical species.[33-35] These reactive species caused oxidative injury inside the bacterial cells, resulting in excellent antibacterial activities of bionanocomposites films.

CONCLUSIONS

Bionanocomposite proton exchange membranes were prepared from sulfonated polybenzimidazole (s-PBI) and various amounts of sulfonated ZnO/cellulose nanohybrids (ZnO/cellulose-SO₃H). Sulfonated ZnO/cellulose nanocomposites were effective additives for preparation of homogeneous s-PBI/ZnO/cellulose-SO₃H

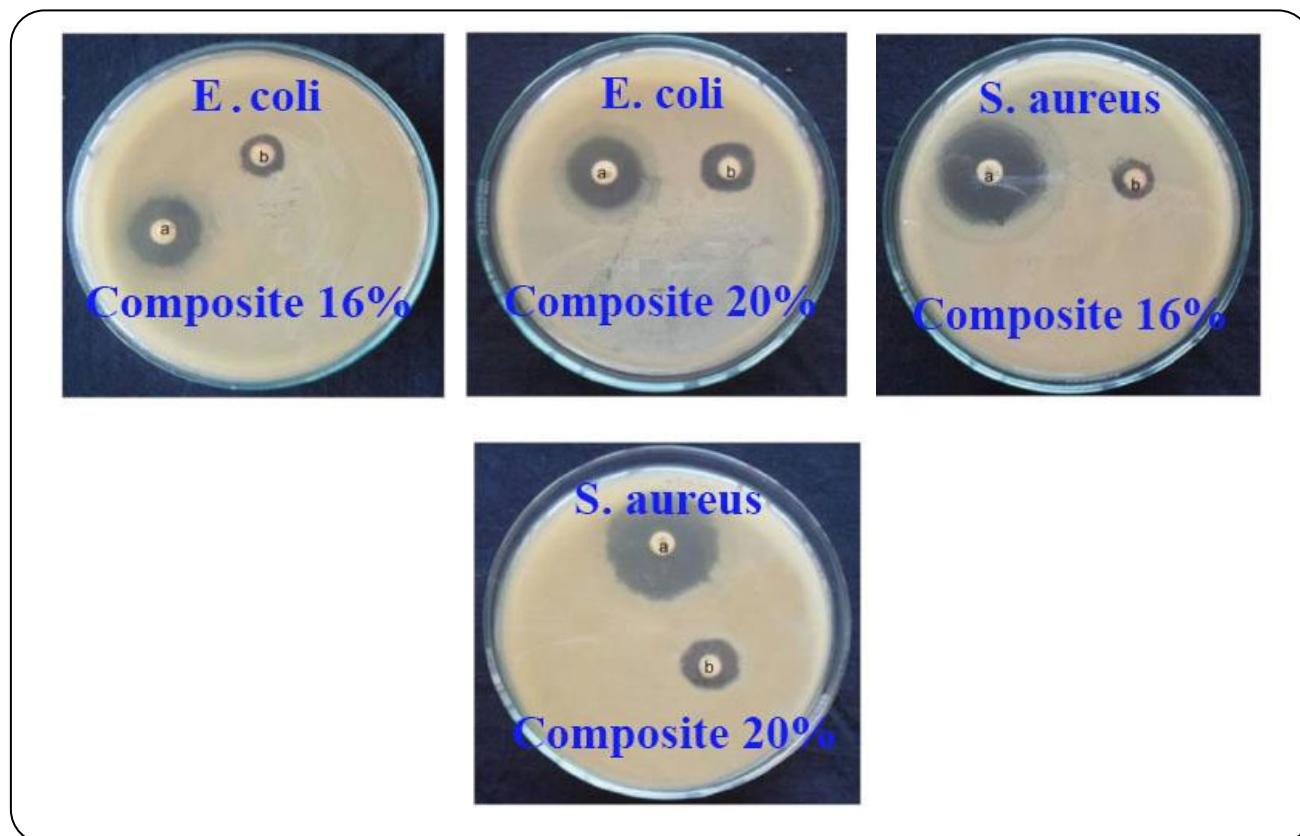


Fig. 11: Inhibition zone test of s-PBI/ZnO/cellulose-SO₃H films against *E. coli* and *S. aureus*.

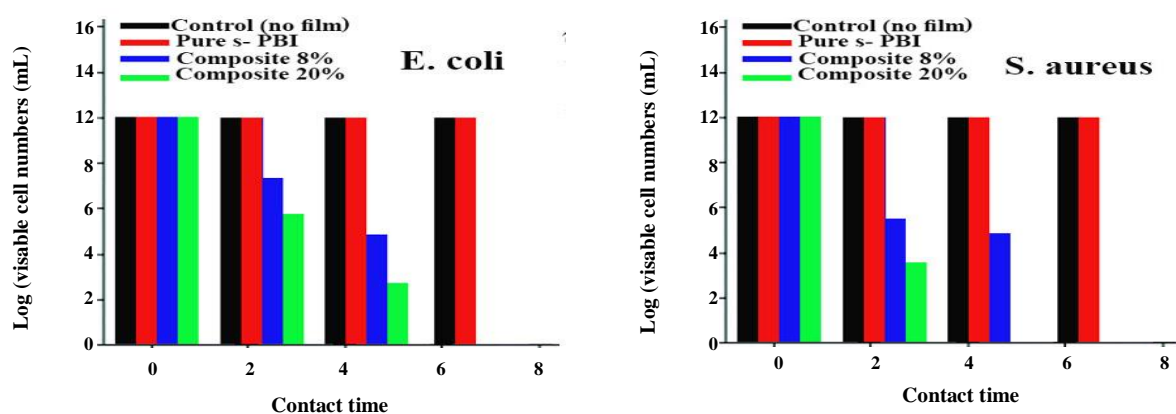


Fig. 12: Viable cell numbers of (a) *E. coli* and (b) *S. aureus* in the control group, s-PBI, s-PBI/ZnO/cellulose-SO₃H (8%) and s-PBI/ZnO/cellulose-SO₃H (20%) films with different contact time.

bionanocomposite membranes. The sulfonic acid groups of ZnO/cellulose-SO₃H enhanced the compatibility between ZnO/cellulose nanocomposites and s-PBI polymer matrix and improved the mechanical properties of the resulting s-PBI/ZnO/cellulose-SO₃H bionanocomposite membranes. Incorporation of

ZnO/cellulose-SO₃H to s-PBI membranes also depressed their methanol permeability and increased their proton conductivities, to result in their high selectivity comparing to pure s-PBI and Nafion[®] membranes. The performances of the s-PBI/ZnO/cellulose-SO₃H bionanocomposite membranes are attractive and

the membrane could be used as proton exchange membranes for direct methanol fuel cells and high temperature/low humidity proton exchange membrane fuel cells. Particularly, s-PBI/ZnO/cellulose-SO₃H bionanocomposite membranes exhibited excellent antibacterial activities against *E. coli* and *S. aureus*. A dramatic reduction in viable bacteria was observed within 4 h of exposure and all of the bacteria were eliminated within 6 h. Therefore, s-PBI/ZnO/cellulose-SO₃H bionanocomposite membranes have significant potential for application in gas separation and fuel cells biomembranes.

Acknowledgments

H. A. acknowledges financial support from Iran Nanotechnology Initiative Council (INIC).

Received: Jan. 21, 2017 ; Accepted : Oct. 16, 2017

REFERENCES

- [1] Wainright J.S., Wang J.-T., Weng D., Savinell R.F., Litt M.H., Acid Doped Polybenzimidazoles: A New Polymer Electrolyte, *J. Electrochem. Soc.*, **142**: L121-L123 (1995).
- [2] Glipa X., Bonnet B., Mula B., Jones D.J., Rozière J., Investigation of the Conduction Properties of Phosphoric and Sulfuric Acid Doped Polybenzimidazole, *J. Mater. Chem.*, **9**: 3045-3049 (1999).
- [3] Ma Y.L., Wainright J.S., Litt M.H., Savinell R.F., Conductivity of PBI membranes for High-Temperature Polymer Electrolyte Fuel Cells, *J. Electrochem. Soc.*, **151**: A8-A16 (2004).
- [4] Li Q., He R., Jensen J.O., Bjerrum N.J., PBI-Based Polymer Membranes for High Temperature Fuel Cells-Preparation, Characterization, and Fuel Cell Demonstration, *Fuel Cells*, **4**: 147-159 (2004).
- [5] Li Q., He R., Berg R.W., Hjulers H.A., Bjerrum N.J., Water Uptake and Doping of Polybenzimidazoles as Electrolyte Membranes for Fuel Cells, *Solid State Ionics*, **168**: 177-185 (2004).
- [6] Asensio J.A., Borrós S., Gómez-Romero P., Polymer Electrolyte Fuel Cells Based on Phosphoric-Acid Impregnated Poly(2,5-benzimidazole) Membranes, *J. Electrochem. Soc.*, **151**: A304-A310 (2004).
- [7] Pu H., Liu Q., Qiao L., Yang Z., Studies on Proton Conductivity of Acid Doped Polybenzimidazole/Polyimide and Polybenzimidazole/Polyvinylpyrrolidone Blends, *Polym. Eng. Sci.*, **45**: 1395-1400 (2005).
- [8] He R., Li Q., Bach A., Jensen J.O., Bjerrum N.J., Physicochemical Properties of Phosphoric Acid Doped Polybenzimidazole Membranes for Fuel Cells, *J. Membr. Sci.*, **277**: 38-45 (2006).
- [9] Lobato J., Cañizares P., Rodrigo M.A., Linares J.J., Aguilar J.A., Improved Polybenzimidazole Films for H₃PO₄-Doped PBI-Based High Temperature PEMFC, *J. Membr. Sci.*, **306**: 47-55 (2007).
- [10] He R., Li Q., Jensen J.O., Bjerrum N.J., Doping Phosphoric Acid in Polybenzimidazole Membranes for High Temperature Proton Exchange Membrane Fuel Cells, *J. Polym. Sci. Part A: Polym. Chem.*, **45**: 2989-2997 (2007).
- [11] Xing B.Z., Savadogo O., The Effect of Acid Doping on the Conductivity of Polybenzimidazole, *J. New Mater. Electrochem. Syst.*, **2**: 95-101 (1999).
- [12] Asensio J.A., Borrós S., Gomez-Romero P., Proton-Conducting Polymers Based on Benzimidazole and Sulfonated Benzimidazole, *J. Polym. Sci. Part A: Polym. Chem.*, **40**: 3703-3710 (2002).
- [13] Qing S., Huang W., Yan D., Synthesis and Characterization of Thermally Stable Sulfonated Polybenzimidazoles Obtained from 3,3-disulfonyl-4,4-dicarboxyldiphenylsulfone, *J. Polym. Sci. Part A: Polym. Chem.*, **43**: 4363-4372 (2005).
- [14] Qing S., Huang W., Yan D., Synthesis and Properties of Soluble Sulfonated Polybenzimidazoles, *React. Funct. Polym.*, **66**: 219-227 (2006).
- [15] Ito A., Hwang S.T., Permeation of Propane and Propylene Through Cellulosic Polymer Membranes, *J. Appl. Polym. Sci.*, **38**: 483-490 (1989).
- [16] Cong H., Radosz M., Towler B.F., Shen Y., Polymer-Inorganic Nanocomposite Membranes for Gas Separation, *Sep. Purif. Technol.*, **55**: 281-291 (2007).
- [17] Joly C., Samaihi M., Porcar L., Noble R.D., Polyimide-Silica Composite Membranes: How Does Silica Influence Their Microstructure and Gas Permeation Properties, *Chem. Mater.*, **11**: 2331-2338 (1999).

- [18] Taherkhani M., [Chemical Investigation and Protective Effects of Bioactive Phytochemicals from *Artemisia Ciniformis*](#), *Iran. J. Chem. Chem. Eng. (IJCCE)*, **35**: 15-26 (2016).
- [19] Biffinger J.C., Ray R., Little B., Ringeisen B.R., [High Power Density from a Miniature Microbial Fuel Cell Using *Shewanella Oneidensis* DSP10](#), *Environ. Sci. Technol.*, **41**: 1444–1449 (2007).
- [20] Wu L., Chen J., Du D., Ju H., [Electrochemical Immunoassay for CA125 Based on Cellulose Acetate Stabilized Antigen/colloidal Gold Nanoparticles Membrane](#), *Electrochim. Acta*, **51**: 1208-1214 (2006).
- [21] Inoue K., Ferrante P., Hirano Y., Yasukawa T., Shiku H., Matsue T., [A Competitive Immunochromatographic Assay for Testosterone Based on Electrochemical Detection](#), *Talanta*, **73**: 886-892 (2007).
- [22] Bonn e M.J., Edler K., Buchanan J.G., Wolverson D., Thielemans W., Psillakis E., Helton M., Marken F., [Thin-Film Modified Electrodes with Reconstituted Cellulose–PDDAC Films for the Accumulation and Detection of Triclosan](#). *J. Phys. Chem. C*, **112**: 2660–2666 (2008).
- [23] Ahmadizadegan H., [Surface Modification of TiO₂ Nanoparticles with Biodegradable Nanocellulose and Synthesis of Novel Polyimide/Cellulose/TiO₂ Membrane](#), *J Colloid Interf Sci*, **491**: 390–400 (2017).
- [24] Liu Y.L., Hsu C.Y., Su Y.H., Lai J.Y., [Chitosan–Silica Complex Membranes from Sulfuric Acid Functionalized Silica Nanoparticles for Pervaporation Dehydration of Ethanol–Water Solutions](#), *Biomacromolecules*, **6**: 368-373 (2005).
- [25] Liu Y., Shi Z., Xu H., Fang J., Ma X., Jin Y., [Preparation, Characterization, and Properties of Novel Polyhedral Oligomeric Silsesquioxane-Polybenzimidazole Nanocomposites by Friedel- Crafts Reaction](#), *Macromolecules*, **43**: 6731-6738 (2010).
- [26] Katepetch C., Rujiravanit R., Tamura H., [Formation of Nanocrystalline ZnO Particles into Bacterial Cellulose Pellicle by Ultrasonic-Assisted in Situ Synthesis](#), *Cellulose*, **20**: 1275-1292 (2013).
- [27] Suryani, Ying-Ling Liu, [Preparation and Properties of Nanocomposite Membranes of Polybenzimidazole/Sulfonated Silica Nanoparticles for Proton Exchange Membranes](#), *J. Membr. Sci.*, **332**: 121-128 (2009).
- [28] Ahmadizadegan H., [Effect of Adding Nanoclay \(Cloisite-30B\) on the Proton Conductivity of Sulfonated Polybenzimidazole](#), *Nanochem Res.*, **2**: 96-108 (2017).
- [29] Liu Y.L., Hsu C.Y., Wei W.L., Jeng R.J., [Preparation and Thermal Properties of Epoxy-Silica Nanocomposites Fromnanoscale Colloidal Silica](#), *Polym*, **44**: 5159-5167 (2003).
- [30] Ahmadizadegan H., [Synthesis and Gas Transport Properties of Novel Functional Polyimide/ZnO Nanocomposite Thin Film Membranes](#) *RSC Adv.*, **6**: 106778-106789 (2016).
- [31] Li C., Sun G., Ren S., Liu J., Wang Q., Wu Z., Sun H., Jin W., [Casting Nafionsulfonated Organosilica Nano-Composite Membranes Used in Direct Methanol Fuel Cells](#), *J. Membr. Sci.*, **272**: 50-57 (2006).
- [32] He R., Li Q., Xiao G., Bjerrum N.J., [Proton Conductivity of Phosphoric Acid Doped Polybenzimidazole and Its Composites with Inorganic Proton Conductors](#), *J. Membr. Sci.*, **226**: 169-184 (2003).
- [33] Fu F., Li L., Liu L., Cai J., Zhang Y., Zhou J., Zhang L., [Construction of Cellulose Based ZnO Nanocomposite Films with Antibacterial Properties Through One-Step Coagulation](#), *ACS Appl. Mater. Interfaces*, **7**: 2597–2606 (2015).
- [34] Singh G., Joyce E.M., Beddow J., Mason T.J., [Evaluation of Antibacterial Activity of ZnO Nanoparticles Coated Sonochemically onto Textile Fabrics](#), *J. Microbiol. Biotechnol. Food Sci.*, **2**: 106-120 (2012).
- [35] Perelshtein I., Ruderman E., Perkas N., Tzanov T., Beddow J., Joyce E., Mason T.J., Blanes M., Molla K., Patlolla A., [Chitosan and Chitosan-ZnO-Based Complex Nanoparticles: Formation, Characterization, and Antibacterial Activity](#), *J. Mater. Chem. B*, **1**: 1968-1976 (2013).
- [36] Anitha S., Brabu B., Thiruvadigal D.J., Gopalakrishnan C., Natarajan T.S., [Optical, Bactericidal and Water Repellent Properties of Electrospun Nano-composite Membranes of Cellulose Acetate and ZnO](#), *Carbohydr. Polym.*, **97**: 855-855 (2013).